

Sharp low energy feature in single-particle spectra due to forward scattering in d -wave cuprate superconductors

Seung Hwan Hong,^{1,*} Jin Mo Bok,^{1,†} Wentao Zhang,² Junfeng He,² X. J. Zhou,² C. M. Varma,³ and Han-Yong Choi^{1,4,‡}

¹*Department of Physics and Institute for Basic Science Research, SungKyunKwan University, Suwon 440-746, Korea.*

²*National Laboratory for Superconductivity, Beijing National Laboratory for Condensed Matter Physics, Institute of Physics, Chinese Academy of Sciences, Beijing 100190, China*

³*Department of Physics and Astronomy, University of California, Riverside, California 92521.*

⁴*Asia Pacific Center for Theoretical Physics, Pohang 790-784, Korea.*

There is an enormous interest in renormalization of quasi-particle (qp) dispersion relation of cuprate superconductors both below and above the critical temperature T_c because it enables determination of the fluctuation spectrum to which the qps are coupled. A remarkable discovery by angle-resolved photoemission spectroscopy (ARPES) is a sharp low energy feature (LEF) in qp spectra well below the superconducting energy gap but with its energy increasing in proportion to T_c and its intensity increasing sharply below T_c . This unexpected feature needs to be reconciled with d -wave superconductivity. Here, we present a quantitative analysis of ARPES data from $\text{Bi}_2\text{Sr}_2\text{CaCu}_2\text{O}_{8+\delta}$ (Bi2212) using Eliashberg equations to show that the qp scattering rate due to the forward scattering impurities far from the Cu-O planes is modified by the energy gap below T_c and shows up as the LEF. This is also a necessary step to analyze ARPES data to reveal the spectrum of fluctuations promoting superconductivity.

PACS numbers: 74.20.-z, 74.25.-q, 74.72.-h

The accumulated high resolution ARPES data on the Bi-cuprate (BSCCO) over a wide doping and temperature range have revealed a sharp feature in the spectral function [1–6]. This occurs below about 10 meV along the nodal $(0,0) - (\pi,\pi)$ direction in the Brillouin zone. Further investigations revealed that the energy of the feature tracks T_c regardless of the families of BSCCO or doping concentration, that its position is much smaller than the maximum energy gap Δ_0 , and that its strength is sharply enhanced below T_c . Here, we show that all these aspects of LEF can be explained by the forward scattering impurities located off the Cu-O planes. We substantiate this by combining computation of the self-energy using the Eliashberg equations and analysis of the momentum distribution curve (MDC) of the ultra high resolution laser based ARPES intensity from Bi2212 in terms of the self-energy [7, 8]. The off-plane impurity parameters from fitting the LEF in the superconducting (SC) state agree well with the normal state scattering rate determined independently as discussed below. This means that the qp scattering rate due to the off-plane impurities is modified by the energy gap below T_c and remarkably shows up as the LEF in the d -wave SC state. The idea that forward scattering in d -wave superconductors may lead to unusual spectroscopic feature in SC state was already pointed out by Zhu, Hirschfeld and Scalapino [9–12]. Here, we quantitatively show the relevance of the idea by analyzing the ARPES experiments at various angles and temperatures to producing the low energy feature. We also compare the off-plane impurity idea with the proposal that the LEF may be due to scattering from

acoustic phonons [13].

The qp scattering rate Γ measured by ARPES in the normal state depends on direction on the Fermi surface and is significantly larger than $k_B T_c$, but this scattering does not show up in the resistivity [14]. This led to the proposal that it is due to dopant impurities which lie in between the Cu-O planes [15]. Such impurities lead only to small angle or forward scatterings for qps near the Fermi surface. The characteristic scattering angle is $\delta\theta \sim a/d$, where a and d are the in-plane and out-of-plane lattice constants. Indeed were this not forward scattering, its effect would exceed the Abrikosov-Gorkov bounds on impurity scattering in d -wave superconductors and there would be no high T_c superconductivity.

The ARPES intensity is given by

$$I(\mathbf{k}, \omega) = |M(\mathbf{k}, \nu)|^2 f(\omega) [A(\mathbf{k}, \omega) + B(\mathbf{k}, \omega)], \quad (1)$$

where M is the matrix element, ν the energy of incident photon, f the Fermi distribution function, $A = -\frac{1}{\pi} \text{Im}[G]$ is the spectral function, and B is the background from the scattering of the photo-electrons. G is the Green's function,

$$G(\mathbf{k}, \omega) = \frac{W + Y}{W^2 - Y^2 - \phi^2}, \quad (2)$$

where $W = \omega - \tilde{\Sigma}(\theta, \omega)$, $Y = \xi(\mathbf{k}) + X(\theta, \omega)$. $\Sigma(\theta, \omega) = \tilde{\Sigma}(\theta, \omega) + X(\theta, \omega)$ is the normal (or, diagonal) self-energy, $\phi(\theta, \omega)$ the anomalous (off-diagonal) self-energy, and $\xi(\mathbf{k})$ is the bare dispersion [8, 16]. We took

$$\begin{aligned} \xi(\mathbf{k}) = & -t[\cos(k_x a) + \cos(k_y a)] - 4t' \cos(k_x a) \cos(k_y a) \\ & - 2t''[\cos(2k_x a) + \cos(2k_y a)] - \mu, \end{aligned} \quad (3)$$

with $t = 0.395$, $t' = 0.084$, $t'' = 0.042$ eV, and $\mu = -0.43$ (UD89K) or -0.48 eV (OD82K). ω stands for the qp energy with respect to the Fermi energy. The in-plane momentum \mathbf{k} is written with the distance from the (π, π) point, k_\perp , and the tilt angle measured from the nodal cut, θ . The MDC analysis fits the measured ARPES intensity using Eqs. (1) and (2) as a function of k_\perp at fixed θ and ω to extract the k_\perp -independent diagonal and off-diagonal self-energies, $\Sigma(\theta, \omega)$ and $\phi(\theta, \omega)$. We note that the dispersion relation from the Lorentzian MDC fitting is not suitable for analyzing off-nodal cuts in SC state because the ARPES dispersion bends back at $\omega \approx -\Delta(\theta)$ due to the gap and meaning of the dispersion relation becomes obscure below $\Delta(\theta)$.

Ultra high resolution laser ARPES data were collected from slightly underdoped Bi2212 of the critical temperature $T_c = 89$ K and pseudogap temperature $T^* \approx 160$ K (denoted by UD89K) and overdoped $T_c = 82$ K Bi2212 samples (OD82K). The experimental setup is the same as in the Ref. 7, 17. The raw ARPES intensity data from UD89K and OD82K together with the extracted self-energy are presented in the supplemental material (SM) [url], which includes Refs. [17, 18].

The qp self-energy may be expressed in terms of two terms, due to coupling to a boson spectrum and to impurities. See below for details. The self-energy from impurity scattering may be written as

$$\Sigma_{imp}(\mathbf{k}, \omega) = n_{imp} \sum_{\mathbf{k}'} \left| V_{imp}(\mathbf{k}, \mathbf{k}') \right|^2 G(\mathbf{k}', \omega), \quad (4)$$

where n_{imp} and V_{imp} are the impurity concentration and impurity potential, respectively. G is the retarded Green's function of Eq. (2) which includes the impurity effects as given by Eq. (11) below. ϕ may also be decomposed similarly with

$$\phi_{imp}(\mathbf{k}, \omega) = -n_{imp} \sum_{\mathbf{k}'} \left| V_{imp}(\mathbf{k}, \mathbf{k}') \right|^2 \frac{\phi(\mathbf{k}', \omega)}{W^2 - Y^2 - \phi^2}. \quad (5)$$

For a momentum independent scattering potential, the self-energy of Eq. (4) at $\mathbf{k} = \mathbf{k}_F$ reduces after integrating over \mathbf{k}' to $\Sigma_{imp}(\omega) = -i\Gamma \langle N(\theta', \omega) \rangle_{\theta'}$, where $N(\theta, \omega) = \omega / \sqrt{\omega^2 - \Delta_0^2 \sin^2(2\theta)}$. After the average over angle $\langle \rangle_{\theta'}$, $\Sigma_{imp}(\omega)$ has an angle independent peak at $\omega = \Delta_0$ below T_c , and it reduces to $\Sigma_{imp} = -i\Gamma$ above T_c as expected. For the strong forward scattering limit of $\theta' \approx \theta$, by contrast,

$$\Sigma_{imp}(\theta, \omega) = -i\Gamma(\theta)N(\theta, \omega), \quad (6)$$

where $\Gamma(\theta) = \pi n_{imp} V_{imp}^2 N_F(\theta)$ and $N_F(\theta) \sim 1/v_F(\theta)$ is the angle dependent DOS at the Fermi surface, so that the impurity self-energy depends on the direction θ .

In Fig. 1(a) we plot the model self-energy of Eq. (6) with a small imaginary part $\Delta_2 = 0.1\Delta_0$. Notice a kink

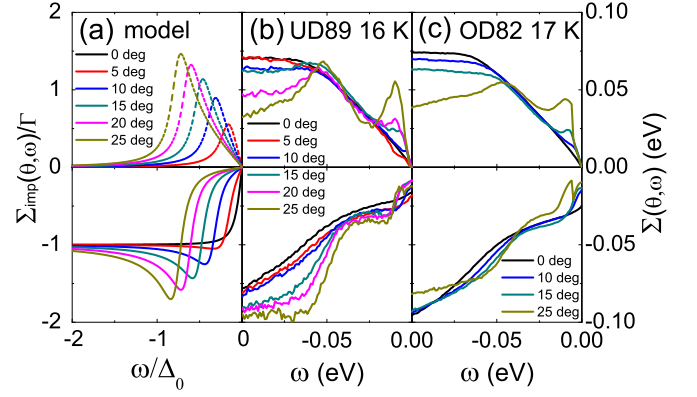


FIG. 1: (a) The impurity self-energy from the model calculation of Eq. (6). The real and imaginary parts are shown along several cuts with the dashed and solid curves, respectively. (b)-(c) The extracted self-energy from MDC analysis of UD89K at $T = 16$ K and of OD82K at $T = 17$ K.

in the self-energy whose position and strength increase as the tilt angle increases. For comparison, we show in Fig. 1(b) and (c) the extracted qp self-energy from the MDC analysis of UD89K and OD82K data in SC state. The LEF shows up below $|\omega| \lesssim 20$ meV. The higher, $\gtrsim 50$ meV, feature is from inelastic coupling to boson fluctuations and will be further discussed below. In agreement with the model calculation, the LEF position in Fig. 1(b) and (c) increases as the tilt angle increases and is smaller than the maximum gap $\Delta_0 \approx 20$ meV. Recall that the peak position in $-\Sigma_2(\mathbf{k}, \omega)$ from coupling to a boson mode of a peak at ω_b (with a broad momentum dependence) is given by $\omega_b + \Delta_0$. [16] The observed feature is impossible to understand with this picture because the observed peak position is less than Δ_0 and angle dependent. But, this feature is naturally understood from the forward scattering off-plane impurities, just as in the normal state.

Now, we consider how the self-energy changes as T varies for a given cut θ . In Fig. 2, we show the imaginary parts of the extracted self-energy from UD89K and OD82K along $\theta = 0$ and $\theta = 15^\circ$. The LEF emerges sharply below T_c and the kink energy increases as T is reduced. Although the LEF is much weaker along the nodal cut compared with off-nodal cuts, we show the nodal cut results to make more concrete contacts with the published reports. [1, 2, 5, 6] For instance, compare Fig. 2(a) and (c) with the inset of Fig. 4(a) in Ref. 6 and notice their similarity. In the normal state it is well established that the ARPES measured scattering rate may be represented as a sum of a constant term and a frequency dependent one as

$$-\Sigma_2(\theta, \omega) = \Gamma(\theta) + b(\theta) \sqrt{\omega^2 + (\pi T)^2}, \quad (7)$$

where the constant Γ is from the off-plane impurities as discussed in the introduction. [15, 19] The frequency de-

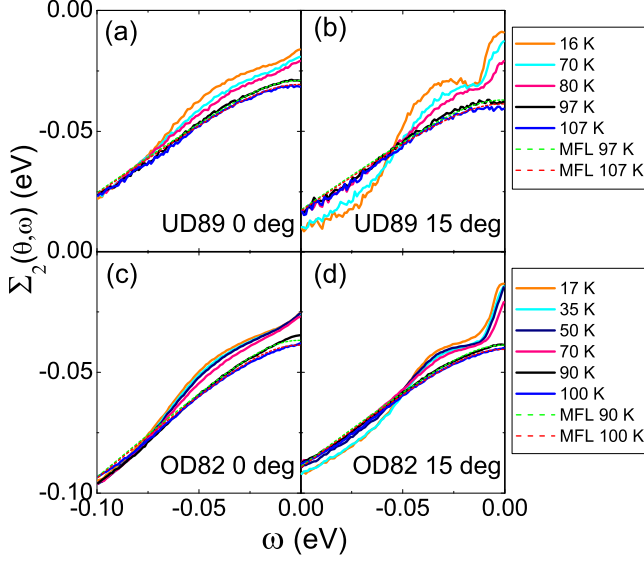


FIG. 2: The imaginary parts of the extracted self-energy from UD89K and OD82K data both above and below T_c along $\theta = 0^\circ$ and 15° . The dashed curves are the fitting from Eq. (7). Notice that the LEF is sharply enhanced below T_c especially along off-nodal cuts.

pendence is well represented by the marginal Fermi liquid (MFL) form[20] as noted previously.[14, 15, 19] The dashed curves in Fig. 2 represent the fitting to Eq. (7). The obtained parameters from the normal state fitting are discussed below in comparison with SC state consideration.

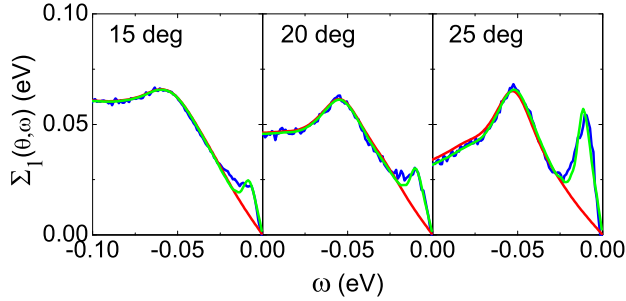


FIG. 3: The real parts of the self-energy of UD89K at 16 K. The blue and green curves represent the extracted and calculated (Eq. (8)) self-energy, and the red curves show the calculated self-energy with the impurity term removed.

We now put the above discussion in a quantitative basis. First, we wish to establish that the LEF mandates the emergence of the zero frequency mode. Because the zero frequency mode represents the impurity term as discussed below, it formally implies that the impurities generate the LEF. This is done by an inversion of the Eliashberg equations. As shown in the SM, the impurity self-

energy may be included in the qp self-energy as the static component of the Eliashberg function $\alpha^2 F^{(+)}(\epsilon' = 0)$ as

$$\Sigma(\theta, \omega) = \int_{-\infty}^{\infty} d\epsilon' M(\omega, \epsilon') \alpha^2 F^{(+)}(\theta, \epsilon'), \quad (8)$$

$$M(\omega, \epsilon') = \int_{-\infty}^{\infty} d\epsilon \frac{f(\epsilon) + n(-\epsilon')}{\epsilon + \epsilon' - \omega - i\delta} \langle \text{Re} N(\theta', \epsilon) \rangle_{\theta'}, \quad (9)$$

where n is the Bose distribution function. Using the MDC extracted $\Sigma(\theta, \omega)$ as an input for the left hand side of the Eq. (8), we may invert this equation to obtain the $\alpha^2 F^{(+)}(\theta, \epsilon')$. The $\alpha^2 F$ so obtained is the fluctuation spectrum for $\epsilon' \neq 0$, and the impurity scattering for $\epsilon' = 0$. The inversion was performed using the maximum entropy method (MEM) as reported previously.[8]

We present in Fig. 3, the extracted $\Sigma_1(\theta, \omega)$ with the blue curves and the calculated self-energy from the MEM inversion of Eq. (8) with the green curves. The strong forward scattering limit was used in the angle averaged DOS in the $M(\omega, \epsilon')$ for $\epsilon' = 0$ of Eq. (9) in the inversion. Then, we removed $\alpha^2 F^{(+)}(\theta, \epsilon' = 0)$ and recalculated the self-energy. The results are shown with the red curves where the LEF is conspicuously absent. This formally establishes that the LEF is due to the forward scattering off-plane impurities. The slight misfit only indicates that the actual impurities in the Bi2212 scatter the electrons more broadly than the extreme forward scattering limit as we show by calculations below.

We now present a second quantitative support for the out-of-plane impurity idea for the LEF with a specific impurity potential. A reasonable model is [9]

$$V_{imp}(\mathbf{k}, \mathbf{k}') = \frac{2\pi\kappa V_0}{[(\mathbf{k} - \mathbf{k}')^2 + \kappa^2]^{3/2}}. \quad (10)$$

κ^{-1} is the range of the impurity potential which controls the angle dependence of the impurity self-energy. We calculated

$$\Sigma(\mathbf{k}, \omega) = \Sigma_{imp}(\mathbf{k}, \omega) - i\Gamma_0,$$

$$\phi(\mathbf{k}, \omega) = \phi_{imp}(\mathbf{k}, \omega) + \phi_0 [\cos(k_x a) - \cos(k_y a)]/2, \quad (11)$$

where the parameters are to be determined by fitting the self-energy quantitatively. Eq. (11) was solved self-consistently together with Eqs. (4) and (5). We compare in Fig. 4 the imaginary parts of the calculated impurity self-energy against that extracted from experiments in UD89K. Fig. 4(a) shows the self-energy as the tilt angle varies at $T = 16$ K, and (b) the temperature evolution at $\theta = 15^\circ$ at $T = 70, 80,$ and 97 K. The comparison of the real part of the self-energy and those from OD82K is presented in SM for completeness. The observed LEF are well reproduced by the off-plane impurity calculations. We stress that the prominent LEF in the self-energy in SC state enables one to accurately determine the parameters of the impurity potential, just like the

electron-phonon interaction function can be most accurately determined in SC state. Of the low energy peak, ϕ_0 determines the energy scale, $n_{imp}V_0^2$ the magnitude, κ the angle dependence of the position, and Γ_0 sets the width. Γ_0 includes the effects of finite temperature and disorder other than the off-plane impurities.

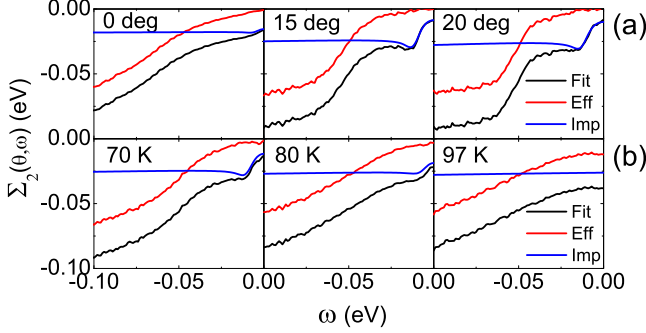


FIG. 4: Comparison of the imaginary parts of the calculated impurity self-energy (blue curves) with the extracted one (black) for UD89K. The red curves represent their difference, that is, the intrinsic self-energy due to coupling to bosons. Figure (a) is as the angle varies at $T = 16$ K, and (b) is as the temperature varies at $\theta = 15^\circ$.

As shown in Fig. 4, we get very good fits to the data. The change of the parameters required in going from UD89K to OD82K is that ϕ_0 decreases from 19 to 16 meV and $n_{imp}V_0^2$ (angle average) from 0.031 to 0.038 $t^2 a \kappa^3$, with t the nearest neighbor hopping amplitude. Other parameters remain almost the same; $\kappa \approx 0.3/a$ and $\Gamma_0 \approx 3$ meV. This is reasonable because $\kappa \sim k_F \delta \theta \sim (1/a)(a/d)$ for off-plane impurity scattering as discussed in the introduction and is expected to be insensitive to doping. But $n_{imp}V_0^2$ is expected to increase with doping and is indeed found larger for OD82K.

The normal state scattering rate from the impurity potential of Eq. (10) in the strong forward scattering limit is given by [9]

$$\Gamma_V(\theta) = -Im\Sigma(\theta, \omega = 0) = \frac{3\pi^2 n_{imp} V_0^2}{8v_F(\theta) \kappa^3}. \quad (12)$$

We calculated Γ_V to check consistency of the idea, using the parameters from deep in SC state (and $\hbar v_F \approx 3.9 - 2.8$ eVÅ for $\theta = 0 - 20^\circ$ from the bare dispersion $\xi(\mathbf{k})$, and the lattice constant $a \approx 3.8$ Å). They are in a good agreement with the $\Gamma(\theta)$ of Eq. (7) from the independent normal state fitting. They are tabulated in detail with other parameters in the Table 1 in the SM. This confirms the idea that the θ -dependent qp scattering rate due to the forward scattering impurities is modified by the energy gap below T_c and shows up as the LEF.

Recently, Johnston *et al.* suggested that the LEF is caused by the acoustic phonons which make forward scatterings due to poor metallicity.[13] κ in this scenario is

set by the Thomas-Fermi wavevector and should increase with doping because of better metallicity. This seems at odds with what is found here. The doping dependence of the LEF has been studied by several groups.[4–6] Ref. 4, 5 reported that the LEF is enhanced as doping is reduced. But, the recent study found that the low energy kink position becomes reduced in the heavily underdoped samples, which seems inconsistent with the acoustic phonon picture.[6] The kink energy in the off-plane impurity scenario is set by the gap and its decrease in the heavily underdoping regime is naturally understood. So is the sharp change of the LEF across T_c because it is given directly by the SC DOS. However, LEF in the acoustic phonon picture is expected to be smoother because it is given by a convolution of DOS and boson spectrum and because it should be present above as well as below T_c since SC is not prerequisite for this effect. Compare the temperature evolution of the boson feature near 50 – 100 meV and the feature near ~ 10 meV of the black curves in Fig. 4(b) and in Fig. 2(b) and (d), and notice the T evolution of the 50 – 100 and ~ 10 meV features is in sharp contrast.

In summary, we have proposed here that the sharp low energy feature observed below ~ 10 meV in BSCCO is indeed caused by the forward scattering off-plane impurities. This conclusion is based on the following observations: (1) the LEF mandates emergence of the Eliashberg spectrum at zero frequency as shown in Fig. 3, (2) the impurity potential well produces the sharp LEF as the angle or temperature is varied as shown in Fig. 4, (3) the parameters of the impurity potential obtained from the SC state satisfactorily match the normal state scattering rates from independent determination, (4) the change of parameters between UD89K and OD82K is consistent with the off-plane impurity idea.

It should be clear by now that the low energy feature of BSCCO ARPES data is from the forward scattering off the out-of-plane impurities. After removing this impurity part from the MDC extracted self-energy we can uncover the intrinsic self-energy as shown by the red curves in Figs. 3 and 4. It is this impurity removed self-energy which must be used as an input to invert the Eliashberg equation. This is a necessary step to reveal the boson spectrum promoting high T_c superconductivity.

Acknowledgments – This work was supported by National Research Foundation (NRF) of Korea through Grant No. NRF-2013R1A1A2061704. XJZ thanks financial support from the NSFC (11190022, 11334010 and 11374335) and the MOST of China (973 program No: 2011CB921703 and 2011CBA00110). CMV's work was supported by NSF-DMR-1206298.

* Present address: School of Computational Sciences, Korea Institute for Advanced Study, Seoul 130-722, Korea.

† Present address: National Laboratory for Superconductivity, Institute of Physics, Chinese Academy of Sciences, Beijing 100190, China

‡ To whom the correspondences should be addressed: hychoi@skku.ac.kr.

- [1] W. Zhang, G. Liu, L. Zhao, H. Liu, J. Meng, X. Dong, W. Lu, J. S. Wen, Z. J. Xu, G. D. Gu, et al., Phys. Rev. Lett. **100**, 107002 (2008).
- [2] N. C. Plumb, T. J. Reber, J. D. Koralek, Z. Sun, J. F. Douglas, Y. Aiura, K. Oka, H. Eisaki, and D. S. Dessau, Phys. Rev. Lett. **105**, 046402 (2010).
- [3] I. M. Vishik, W. S. Lee, F. Schmitt, B. Moritz, T. Sasagawa, S. Uchida, K. Fujita, S. Ishida, C. Zhang, T. P. Devereaux, et al., Phys. Rev. Lett. **104**, 207002 (2010).
- [4] H. Anzai, A. Ino, T. Kamo, T. Fujita, M. Arita, H. Namatame, M. Taniguchi, A. Fujimori, Z.-X. Shen, M. Ishikado, et al., Phys. Rev. Lett. **105**, 227002 (2010).
- [5] T. Kondo, Y. Nakashima, W. Malaeb, Y. Ishida, Y. Hamaya, T. Takeuchi, and S. Shin, Phys. Rev. Lett. **110**, 217006 (2013).
- [6] Y. Peng, J. Meng, L. Zhao, Y. Liu, J. He, G. Liu, X. Dong, S. He, J. Zhang, C. Chen, et al., Chin. Phys. Lett. **6**, 067402 (2013).
- [7] W. Zhang, J. M. Bok, J. H. Yun, J. He, G. Liu, L. Zhao, H. Liu, J. Meng, X. Jia, Y. Peng, et al., Phys. Rev. B **85**, 064514 (2012).
- [8] J. H. Yun, J. M. Bok, H.-Y. Choi, W. Zhang, X. J. Zhou, and C. M. Varma, Phys. Rev. B **84**, 104521 (2011).
- [9] L. Zhu, P. J. Hirschfeld, and D. J. Scalapino, Phys. Rev. B **70**, 214503 (2004).
- [10] D. Scalapino, T. Nunner, and P. Hirschfeld, J. Phys. Chem. Solids **67**, 6 (2006).
- [11] T. Dahm, P. J. Hirschfeld, L. Zhu, and D. J. Scalapino, Phys. Rev. B **71**, 212501 (2005).
- [12] S. Graser, P. J. Hirschfeld, L.-Y. Zhu, and T. Dahm, Phys. Rev. B **76**, 054516 (2007).
- [13] S. Johnston, I. M. Vishik, W. S. Lee, F. Schmitt, S. Uchida, K. Fujita, S. Ishida, N. Nagaosa, Z. X. Shen, and T. P. Devereaux, Phys. Rev. Lett. **108**, 166404 (2012).
- [14] T. Valla, A. V. Fedorov, P. D. Johnson, B. O. Wells, S. L. Hulbert, Q. Li, G. D. Gu, and N. Koshizuka, Science **285**, 2110 (1999).
- [15] E. Abrahams and C. Varma, Proc. Nat. Acad. Sci. **97**, 5714 (2000).
- [16] A. W. Sandvik, D. J. Scalapino, and N. E. Bickers, Phys. Rev. B **69**, 094523 (2004).
- [17] J. He, W. Zhang, J. M. Bok, D. Mou, L. Zhao, Y. Peng, S. He, G. Liu, X. Dong, J. Zhang, et al., Phys. Rev. Lett. **111**, 107005 (2013).
- [18] H. Matsui, T. Sato, T. Takahashi, S.-C. Wang, H.-B. Yang, H. Ding, T. Fujii, T. Watanabe, and A. Matsuda, Phys. Rev. Lett. **90**, 217002 (2003).
- [19] A. Kaminski, H. M. Fretwell, M. R. Norman, M. Randeria, S. Rosenkranz, U. Chatterjee, J. C. Campuzano, J. Mesot, T. Sato, T. Takahashi, et al., Phys. Rev. B **71**, 014517 (2005).
- [20] C. M. Varma, P. B. Littlewood, S. Schmitt-Rink, E. Abrahams, and A. E. Ruckenstein, Phys. Rev. Lett. **63**, 1996 (1989).

Supplemental Material for Sharp low energy feature in single-particle spectra due to forward scattering in d -wave cuprate superconductors

Seung Hwan Hong* and Jin Mo Bok†

*Department of Physics and Institute for Basic Science Research,
SungKyunKwan University, Suwon 440-746, Korea.*

Wentao Zhang, Junfeng He, and X. J. Zhou

*National Laboratory for Superconductivity, Beijing National Laboratory for Condensed Matter Physics,
Institute of Physics, Chinese Academy of Sciences, Beijing 100190, China*

C. M. Varma

Department of Physics and Astronomy, University of California, Riverside, California 92521.

Han-Yong Choi‡

*Department of Physics and Institute for Basic Science Research,
SungKyunKwan University, Suwon 440-746, Korea. and
Asia Pacific Center for Theoretical Physics, Pohang 790-784, Korea.*

PACS numbers:

ARPES intensity and MDC self-energy analysis

The ARPES measurements were performed on the vacuum ultraviolet (VUV) laser-based angle-resolved photoemission system with advantages of high photon flux, enhanced bulk sensitivity, and super-high energy and momentum resolution. The photon energy is 6.994 eV with a bandwidth of 0.26 meV. We set the energy resolution of the electron energy analyzer (Scienta R4000) at 1 meV, giving rise to an overall energy resolution of 1.03 meV. The angular resolution is $\sim 0.3^\circ$, corresponding to a momentum resolution of $\sim 0.004 \text{ \AA}^{-1}$ for the 6.994 eV photon energy. The experimental setup is the same as the Ref. 1, 2. The ultra high resolution laser ARPES data were collected from slightly underdoped Bi2212 of the critical temperature $T_c = 89 \text{ K}$ and pseudogap temperature $T^* \approx 160 \text{ K}$ (denoted by UD89K) and overdoped $T_c = 82 \text{ K}$ Bi2212 samples (OD82K).

We present in Fig. 1 the raw ARPES intensity from UD89K at $T = 16 \text{ K}$ in the first row and OD82K at $T = 17 \text{ K}$ in the second row. In Fig. 2 we show the dispersion relation and scattering rate (a1-a6 for UD89K and c1-c6 for OD82K) and the real and imaginary parts of the self-energy (b1-b6 for UD89K and d1-d6 for OD82K). The dispersion relation and scattering rate were obtained from the Lorentzian fitting of the momentum distribution curves (MDC), and the self-energy from the MDC fitting using the full SC Green's function as explained in the main text. The discrepancy between a and b and between c and d comes from the fact that the tight-binding dispersion and the full SC Green's function were used in the Green's function fitting. The Lorentzian fitting amount to using linear dispersion. The difference between a1 and b1 along the nodal cut arises only because the tight-binding bare dispersion was employed in the self-energy analysis.

As the tilt angle increases away from the nodal direction, the shallower band bottom can be described using the tight-binding dispersion which however is entirely missed by the linear dispersion. Also, the ARPES dispersion bends back at $\omega \approx -\Delta(\theta)$ due to pairing [1, 3] and meaning of the dispersion relation is not clear below the gap energy, which becomes pronounced for large tilt angle. As Zhu *et al.* pointed out, the near cancellation of the sharp features in the diagonal and off-diagonal self-energies substantially weakens the feature in the scattering rate.[4] For instance, compare a6 and b6 of UD89K at $\theta = 25^\circ$ and $T = 16 \text{ K}$. The dispersion relation and scattering rate in a6 show qualitatively different behavior below $\sim 20 \text{ meV}$ from the self-energy in b6. They can be misleading as explained above. On the other hand, the self-energy is well defined for all θ and ω , and we will discuss the LEF in terms of

*Present address: School of Computational Sciences, Korea Institute for Advanced Study, Seoul 130-722, Korea.

†Present address: National Laboratory for Superconductivity, Institute of Physics, Chinese Academy of Sciences, Beijing 100190, China

‡To whom the correspondences should be addressed: hychoi@skku.ac.kr.

the self-energy from the MDC analysis using the full SC Green's function. The LEF shows up more clearly along off-nodal cuts as can be seen from the plots in Fig. 1 and 2, and should be analyzed there properly.

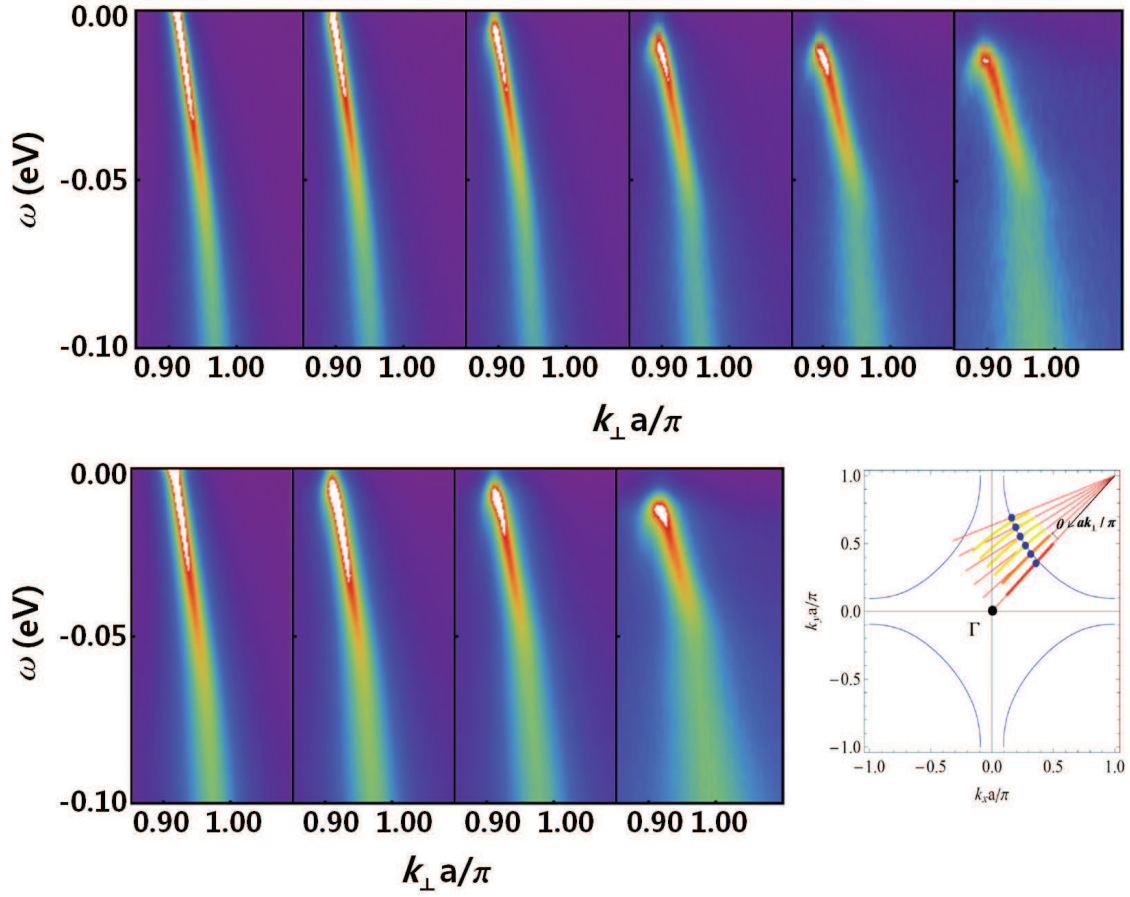


FIG. 1: The raw ARPES intensity from the UD89K and OD82K. The first and second rows are the intensity from UD89K at $T = 16$ K and OD82K at $T = 17$ K, respectively. The tilt angle for the first row is 0, 5, 10, 15, 20, and 25 deg from the left, and for the second row, the angle is 0, 10, 15, 25 deg. In the right corner, the Fermi surface of Bi2212 is illustrated where k_{\perp} is the distance from the (π, π) point in the Brillouin zone and θ is the tilt angle from the $(0, 0) - (\pi, \pi)$ nodal direction.

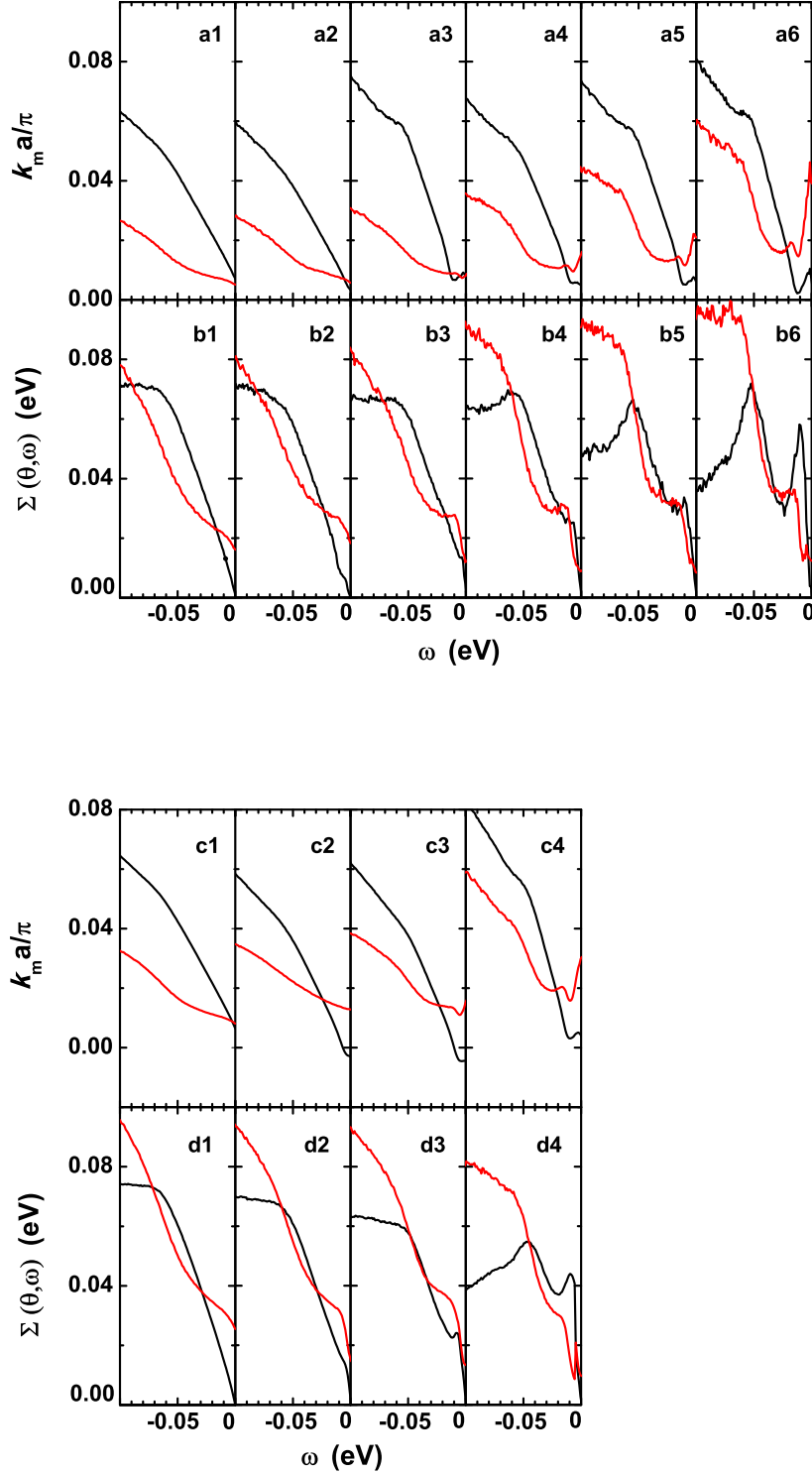


FIG. 2: (a) & (b) Analysis of the ARPES intensity of UD89K shown in Fig. 1. (a) The dispersion relation and scattering rate (HWHM) determined from the Lorentzian MDC fitting, shown in the black and red, respectively. $k_m = k_{\perp}^{max} - k_0$, where k_{\perp}^{max} is the distance from the (π, π) to the maximum point where the MDC has a peak in the BZ and k_0 is the distance from (π, π) to the Fermi surface along a given angle. The tilt angles are the same order as in Fig. 1. (b) The real and imaginary parts of the self-energy determined from the MDC fitting with the full SC Green's function as explained in the main text. The black and red show the real part $\Sigma_1(\theta, \omega)$ and minus of the imaginary part $-\Sigma_2(\theta, \omega)$ as a function of ω . (c) & (d) Analysis of OD82K intensity of Fig. 1. (c) The dispersion relation and scattering rate of OD82K at $T = 17$ K along $\theta = 0, 10, 15$, and 25° from left. (d) The $\Sigma_1(\theta, \omega)$ in black and $-\Sigma_2(\theta, \omega)$ in red of OD82K at $T = 17$ K. The small spiky feature of the red curve in d4 near ~ 5 meV is from a numerical instability and should be disregarded.

Eliashberg theory with boson and impurity

The qp self-energy may be decomposed into two contributions as

$$\Sigma(\mathbf{k}, \omega) = \Sigma_{eff}(\mathbf{k}, \omega) + \Sigma_{imp}(\mathbf{k}, \omega). \quad (1)$$

The first and second parts come from coupling to a boson spectrum and to impurities, respectively, and may be written as

$$\Sigma_{eff}(\mathbf{k}, \omega) = \int_{-\infty}^{\infty} d\varepsilon \int_{-\infty}^{\infty} d\varepsilon' \frac{f(\varepsilon) + n(-\varepsilon')}{\varepsilon + \varepsilon' - \omega - i\delta} \sum_{\mathbf{k}'} A(\mathbf{k}', \varepsilon) \alpha^2 F^{(+)}(\mathbf{k}, \mathbf{k}', \varepsilon'), \quad (2)$$

$$\Sigma_{imp}(\mathbf{k}, \omega) = n_{imp} \sum_{\mathbf{k}'} \left| V_{imp}(\mathbf{k}, \mathbf{k}') \right|^2 G(\mathbf{k}', \omega), \quad (3)$$

where f and n are the Fermi and Bose distribution functions, respectively, δ an positive infinitesimal number, and $\alpha^2 F^{(+)}$ is the diagonal Eliashberg function. The n_{imp} and V_{imp} are the impurity concentration and impurity potential energy, respectively. The anomalous self-energy ϕ may also be decomposed similarly as [4]

$$\Sigma(\mathbf{k}, \omega) = \Sigma_{eff}(\mathbf{k}, \omega) + \Sigma_{imp}(\mathbf{k}, \omega), \quad (4)$$

where the first and second terms are from the coupling to the boson and impurities, as before, and may be written as

$$\phi_{eff}(\mathbf{k}, \omega) = - \int_{-\infty}^{\infty} d\varepsilon \int_{-\infty}^{\infty} d\varepsilon' \frac{f(\varepsilon) + n(-\varepsilon')}{\varepsilon + \varepsilon' - \omega - i\delta} \sum_{\mathbf{k}'} A_{\phi}(\mathbf{k}', \varepsilon) \alpha^2 F^{(-)}(\mathbf{k}, \mathbf{k}', \varepsilon'), \quad (5)$$

$$\phi_{imp}(\mathbf{k}, \omega) = -n_{imp} \sum_{\mathbf{k}'} \left| V_{imp}(\mathbf{k}, \mathbf{k}') \right|^2 G_{\phi}(\mathbf{k}', \omega), \quad (6)$$

where $\alpha^2 F^{(-)}$ is the off-diagonal Eliashberg function, and

$$A_{\phi}(\mathbf{k}, \omega) = -\frac{1}{\pi} \text{Im} [G_{\phi}(\mathbf{k}, \omega)], \quad G_{\phi}(\mathbf{k}, \omega) = \frac{\phi(\mathbf{k}, \omega)}{W^2 - Y^2 - \phi^2}. \quad (7)$$

Now, by the symmetry requirement of

$$\alpha^2 F(-\epsilon') = -\alpha^2 F(\epsilon'), \quad (8)$$

we have $\alpha^2 F(\epsilon' = 0) = 0$. But, the $n(\epsilon')$ in Eq. (2) diverges as $\epsilon' \rightarrow 0$, and the product $\alpha^2 F(\epsilon')n(\epsilon')$ can be finite, which may represent the impurity term as follows. Use $n(-\epsilon') = -[n(\epsilon') + 1]$, Eq. (8), and

$$F(\omega) = \frac{1}{\pi} \int_{-\infty}^{\infty} d\epsilon \frac{1}{\epsilon - \omega - i\delta} \text{Im} F(\epsilon), \quad (9)$$

to separate the $\epsilon' \rightarrow 0$ term out from Eq. (2) as

$$\Sigma_{eff}(\mathbf{k}, \omega) = \sum_{\mathbf{k}'} G(\mathbf{k}', \omega) \alpha^2 F_0(\mathbf{k}, \mathbf{k}'), \quad (10)$$

$$\alpha^2 F_0(\mathbf{k}, \mathbf{k}') \equiv \lim_{f \rightarrow 0} s \coth(sf/2T) \alpha^2 F^{(+)}(\mathbf{k}, \mathbf{k}', sf), \quad (11)$$

where s is the step size of numerical integration, and the infinitesimal $\epsilon' \rightarrow 0$ is written as $\epsilon' = sf$. Comparing Eq. (10) with (3) we have

$$n_{imp} \left| V_{imp}(\mathbf{k}, \mathbf{k}') \right|^2 = \alpha^2 F_0(\mathbf{k}, \mathbf{k}'). \quad (12)$$

This means that if we take the zero frequency limit of the Eliashberg function such that

$$\lim_{f \rightarrow 0} \alpha^2 F^{(+)}(\mathbf{k}, \mathbf{k}', sf) = \frac{f}{2T} n_{imp} \left| V_{imp}(\mathbf{k}, \mathbf{k}') \right|^2, \quad (13)$$

the impurity potential term may be expressed as the zero frequency component of the boson spectrum. That is, the self-energy of Eq. (1) may be written as

$$\Sigma(\mathbf{k}, \omega) = \int_{-\infty}^{\infty} d\varepsilon \int_{-\infty}^{\infty} d\varepsilon' \frac{f(\varepsilon) + n(-\varepsilon')}{\varepsilon + \varepsilon' - \omega - i\delta} \sum_{\mathbf{k}'} A(\mathbf{k}', \varepsilon) \alpha^2 F^{(+)}(\mathbf{k}, \mathbf{k}', \varepsilon'), \quad (14)$$

together with Eq. (13).

In order to calculate the Eliashberg function $\alpha^2 F^{(+)}$, we perform the k_{\perp}' summation of \mathbf{k}' using

$$\begin{aligned} \int dk_{\perp}' A(\mathbf{k}', \epsilon) &= \frac{1}{\hbar v_F(\theta')} \text{Re} N(\theta', \epsilon), \\ N(\theta', \epsilon) &= \frac{\epsilon}{\sqrt{\epsilon^2 - \Delta^2(\theta', \epsilon)}}, \end{aligned} \quad (15)$$

and rewrite Eqs. (14) as

$$\Sigma(\theta, \omega) = \int_{-\infty}^{\infty} d\epsilon' M(\omega, \epsilon') \alpha^2 F^{(+)}(\theta, \epsilon'), \quad (16)$$

where

$$M(\omega, \epsilon') = \int_{-\infty}^{\infty} d\epsilon \frac{f(\epsilon) + n(-\epsilon')}{\epsilon + \epsilon' - \omega - i\delta} \langle \text{Re} N(\theta', \epsilon) \rangle_{\theta'}, \quad (17)$$

$$\alpha^2 F^{(+)}(\theta, \omega) = \left\langle \frac{\alpha^2(\theta, \theta')}{v_F(\theta')} F^{(+)}(\theta, \theta', \omega) \right\rangle_{\theta'}. \quad (18)$$

Then, using the MDC extracted self-energy as an input (the left hand side of Eq. (16)), the Eliashberg function $\alpha^2 F^{(+)}(\theta, \omega)$ may be straightforwardly obtained by inverting this equation. The inversion was performed using the maximum entropy method (MEM).

The self-energy and parameters of impurity potential

As explained in the main text the low energy feature in the ARPES experiments in BSCCO was modeled by the off-plane impurity potential. The fitting of the imaginary part of the self-energy from UD89K with the impurity potential was presented in the main text. We here show for completeness the plots of fitting the real part of the self-energy of UD89K and the real and imaginary parts of the self-energy from OD82K in Fig. 3.

The parameters obtained from the fitting of UD89K and OD82K are listed in Table 1. $\Gamma(\theta)$ and $\Gamma_V(\theta)$ are from Eqs. (7) and (12), respectively.

TABLE I: Parameters of the impurity potential from fitting the self-energy of UD89K and OD82K as shown in Fig. 4 of the main text and Fig. 3 of the SM. The $\Gamma(\theta)$ and $\Gamma_V(\theta)$ are the estimates from Eqs. (7) and (12), respectively.

	UD89K at 16 K			OD82K at 17 K		
θ (deg)	0	15	20	0	10	15
κ ($1/a$)	0.3	0.3	0.3	0.3	0.3	0.3
$n_{imp} V_0^2$ ($t^2 a \kappa^3$)	0.03	0.033	0.03	0.045	0.035	0.035
Γ_0 (meV)	1.5	2.5	3.5	2.5	3.0	3.3
ϕ_0 (meV)	20	20	18	16	16	16
Γ (meV)	13	21	23	19	20	23
Γ_V (meV)	17	23	24	26	22	24

[1] W. Zhang, J. M. Bok, J. H. Yun, J. He, G. Liu, L. Zhao, H. Liu, J. Meng, X. Jia, Y. Peng, et al., Phys. Rev. B **85**, 064514 (2012).

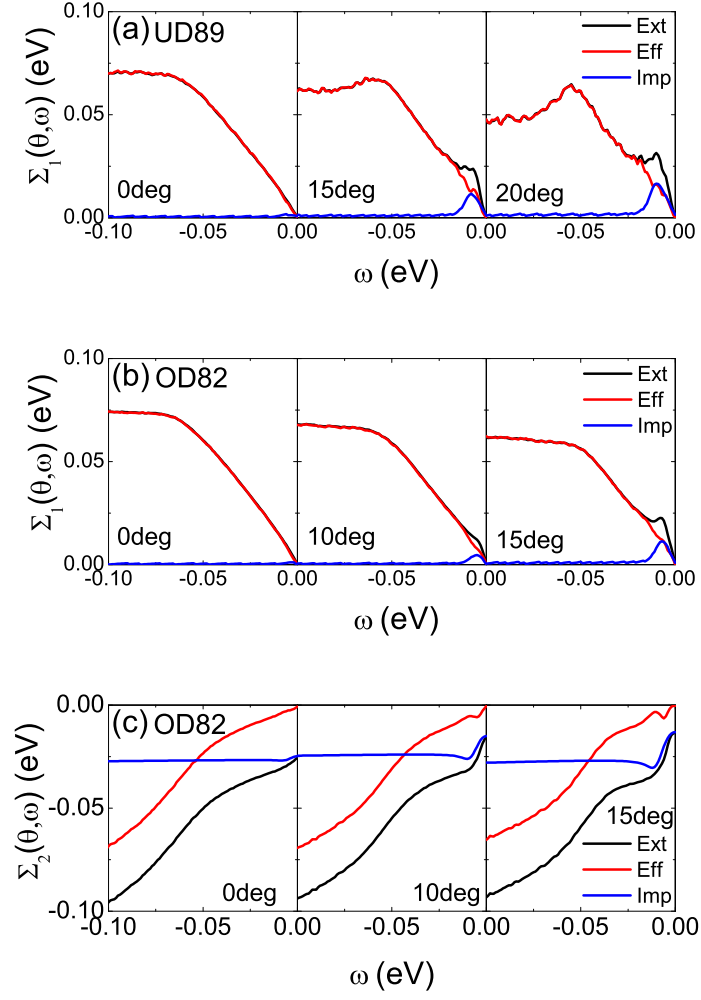


FIG. 3: Comparison of the calculated impurity self-energy (blue curves) with the MDC deduced one (black) for UD89K, as explained in the main text. The red curves represent their difference, that is, the Σ_{eff} due to the coupling to bosons. Figure (a) is the comparison of the real parts of UD89K at 16 K, and (b) & (c) are, respectively, comparison of the real and imaginary parts of the OD82K at 17 K.

- [2] J. He, W. Zhang, J. M. Bok, D. Mou, L. Zhao, Y. Peng, S. He, G. Liu, X. Dong, J. Zhang, et al., Phys. Rev. Lett. **111**, 107005 (2013).
- [3] H. Matsui, T. Sato, T. Takahashi, S.-C. Wang, H.-B. Yang, H. Ding, T. Fujii, T. Watanabe, and A. Matsuda, Phys. Rev. Lett. **90**, 217002 (2003).
- [4] L. Zhu, P. J. Hirschfeld, and D. J. Scalapino, Phys. Rev. B **70**, 214503 (2004).